Supplementary Information (SI) for Sustainable Energy & Fuels.
This journal is © The Royal Society of Chemistry 2024

Intermittent control switch characteristics of triboelectric electric hybrid energy harvesting devices and power management circuits

Xin Yu [a], Mingxing Cui [a], Wendong Qi [a], Xinrui Li [a], Yuhang Xing [a] , Xiaolei Lu [a], ,Shitong Yang [b] , Jing Zhao [a,] *, Changhong Jiang [a,] *

[a] *School of Electrical and Electronic Engineering, Changchun University of Technology, Changchun, Jilin 130012, China.*
[b] *School of Mechatronic Engineering, Changchun University of Technology, Changchun, Jilin 130012, China*

* Corresponding authors' e-mail addresses: zhaojing@ccut.edu.cn; yuxinnick@ccut.edu.cn

Support pictures

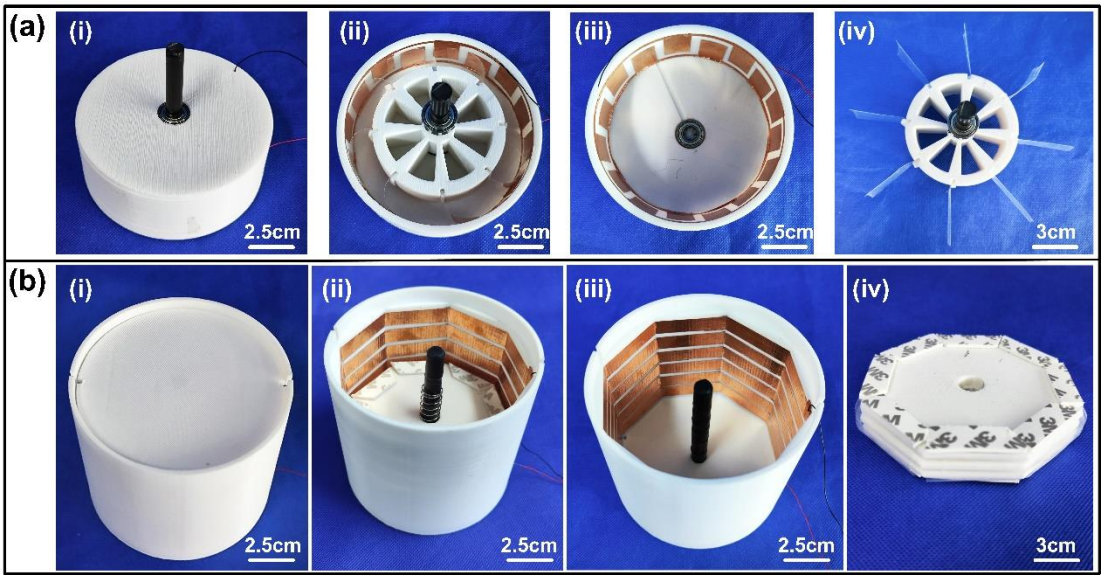

Figure S1. HEH-TENG actual photographs. (a) R-TENG actual photographs (i) overall picture, (ii) internal photograph, (iii) stator photograph and (iv) rotor photograph. (b)V-TENG actual photographs (i) overall picture, (ii) internal photograph, (iii) stator photograph and (iv) vibrating block photograph.

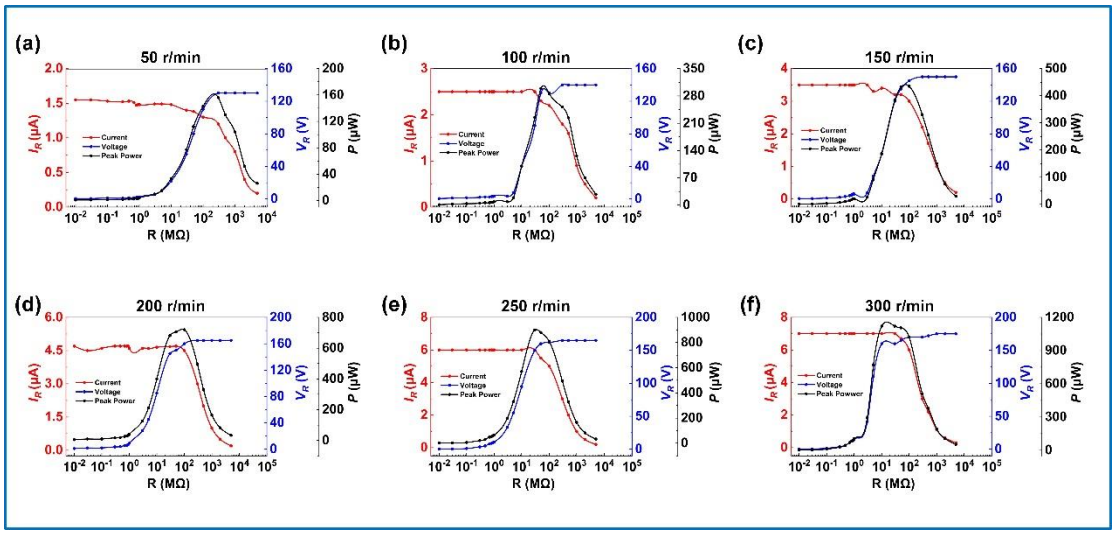

Figure S2. The waveforms of open-circuit voltage, short-circuit current and peak power output by R-TENG under different resistance loads at different speeds.

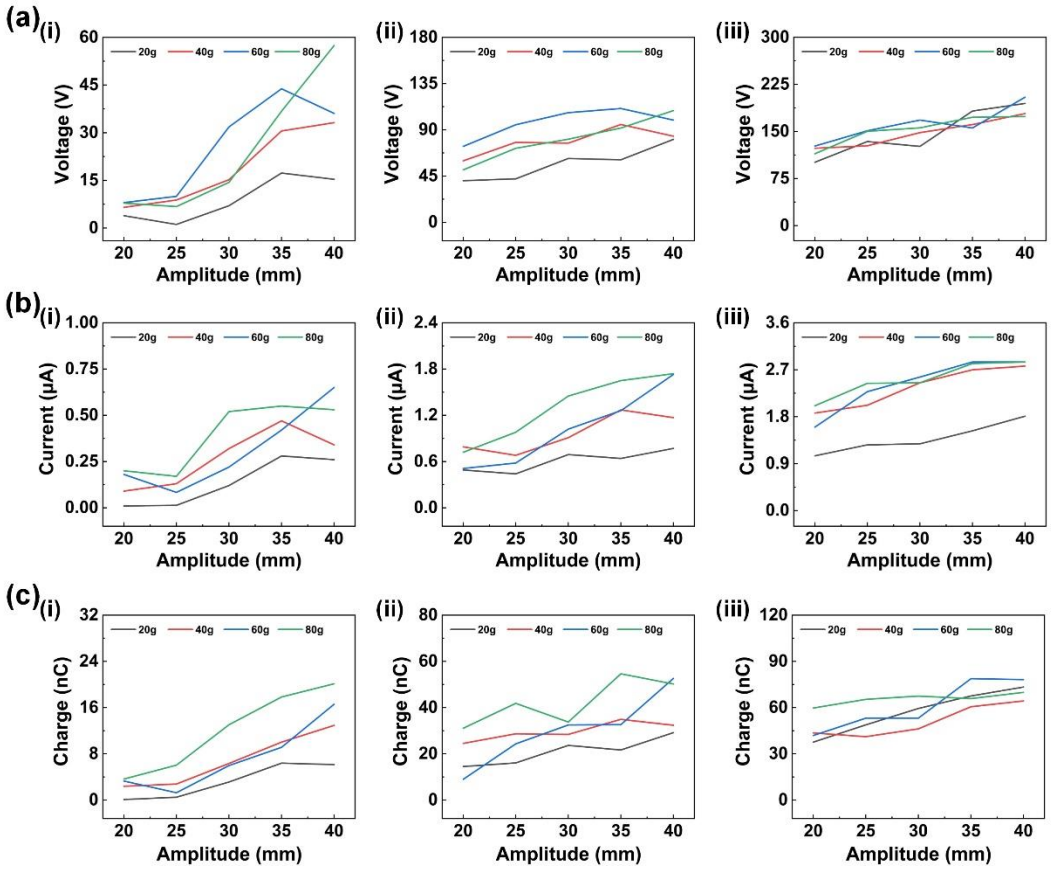

Figure S3. Open-circuit voltage, short-circuit current and transferred charge of V-TENG at different amplitudes of the same frequency. (a) In (i), (ii) and (iii) are the open-circuit voltages of V-TENG at different amplitudes at frequencies of 1.5 hz, 2.0 hz and 2.5 hz, respectively. (b) in (i), (ii) and (iii) are the short-circuit currents of the V-TENG for different amplitudes at frequencies of 1.5 hz, 2.0 hz and 2.5 hz, respectively. (c) In (i), (ii) and (iii) are the transferred charges of V-TENG with different amplitudes at frequencies of 1.5 hz, 2.0 hz and 2.5 hz,

respectively.

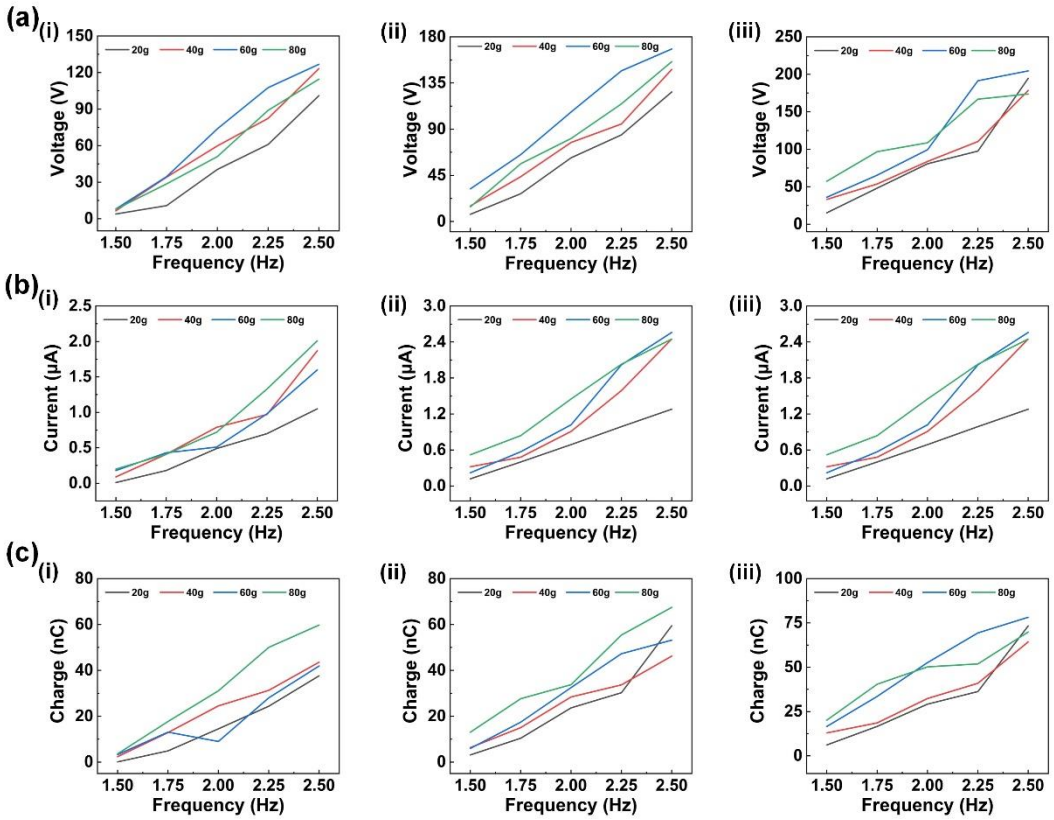

Figure S4. Open-circuit voltage, short-circuit current and transferred charge of V-TENG at different frequencies for the same value. In (a) (i), (ii) and (iii) are the open-circuit voltages of V-TENG at different frequencies for amplitudes of 20 mm, 30 mm and 40 mm, respectively. (b) in (i), (ii) and (iii) are the short-circuit currents of the V-TENG at different frequencies for amplitudes of 20 mm, 30 mm and 40 mm, respectively. (c) in (i), (ii) and (iii) are the transferred charges of V-TENG at different frequencies for amplitudes of 20 mm, 30 mm and 40 mm, respectively.

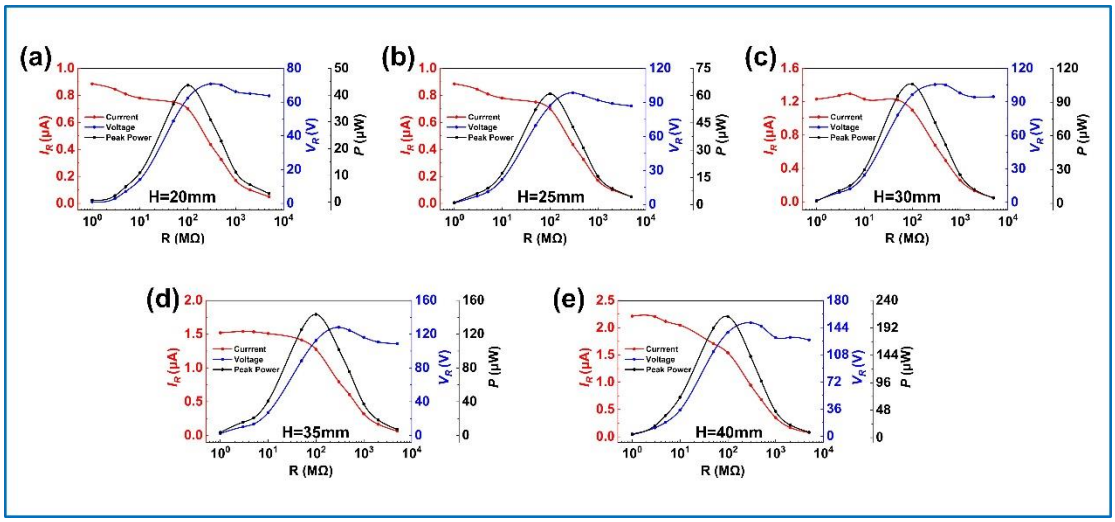

Figure S5. The open-circuit voltage, short-circuit current and peak power of V-TENG output under different resistance loads are plotted under different amplitudes at a fixed frequency of

2.25 Hz.

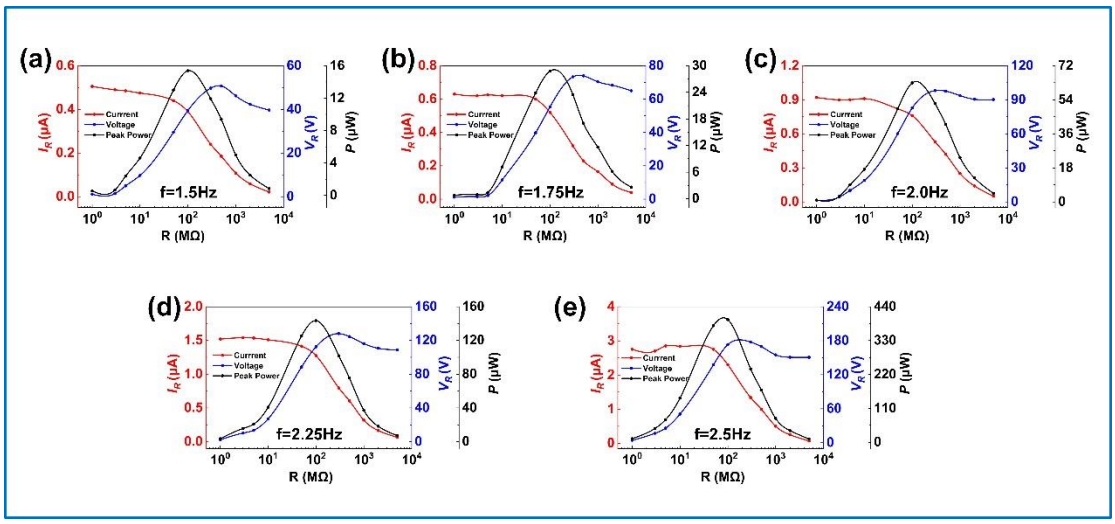

Figure S6. At a fixed vibration amplitude of 35 mm, the open circuit voltage, short circuit current and peak power of V-TENG output under different resistance loads at different frequencies are plotted.

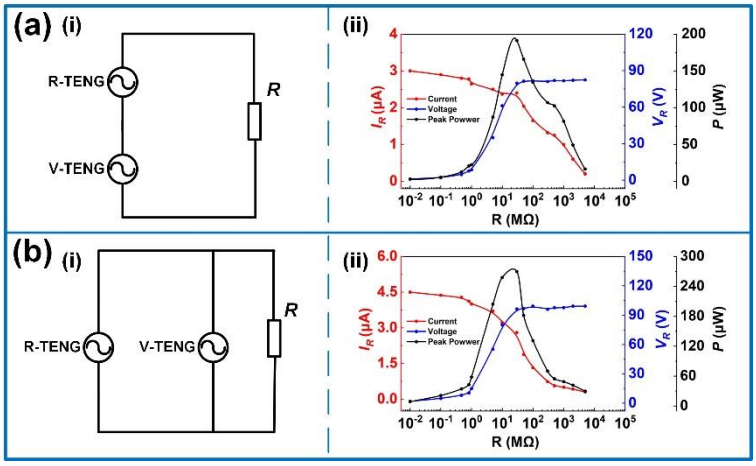

Figure S7. R-TENG and V-TENG series and parallel circuit diagram and series and parallel corresponding impedance matching diagram.

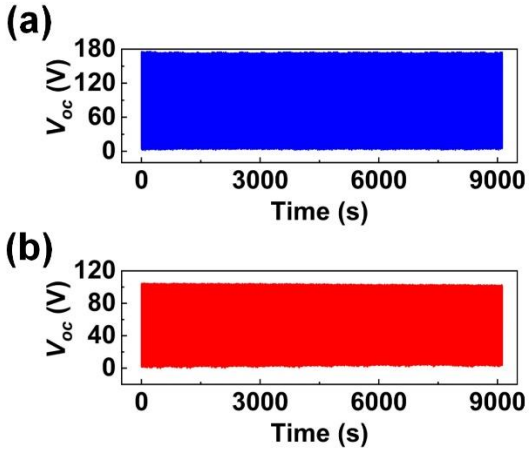

Figure S8. Open-circuit voltage plot of R-TENG running for 9000 s. (b) Open-circuit voltage plot of V-TENG running for 9000 s.

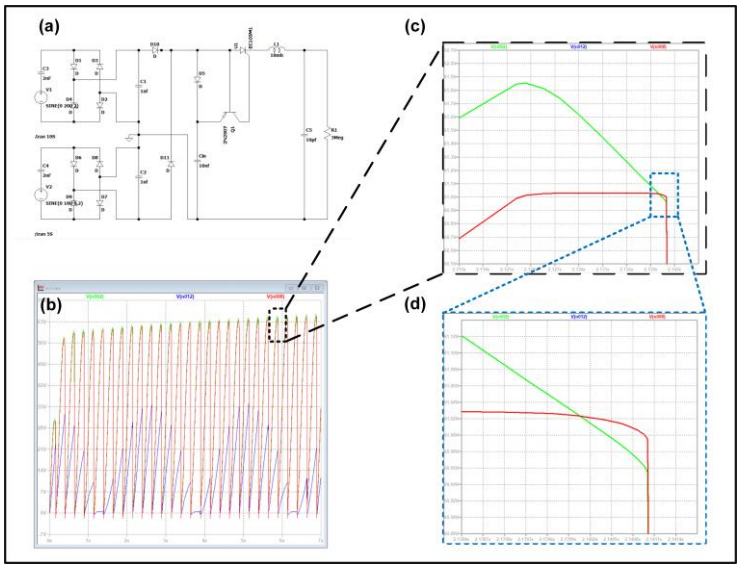

Figure S9 The voltage simulation diagram of the detection capacitor C_{in} and the storage capacitors C_1 and C_2 when HEH-TENG is running. (a) Simulation circuit diagram. (b) The overall voltage waveform. (c) and (d) are voltage waveform amplification diagrams.

The simulation diagram is shown in Fig. S9, where Fig. (a) is the circuit diagram drawn in the simulation software. Figure (b) is the real-time voltage waveform of the storage capacitor C_1, C_2 and the detection capacitor C_{in}. In the (b) diagram, the green and red curves are the voltage waveforms of the detection capacitor C_{in} and the storage capacitor C_1, respectively, and the blue curve is the voltage waveform of the storage capacitor C_2. When HEH-TENG is working, due to the high output power and frequency of R-TENG, the voltage of the detection capacitor is equal to the voltage rise speed of the storage capacitor C_1, and the two curves almost overlap in the simulation diagram. The output power and frequency of V-TENG are low, and the storage capacitor C_2 is slowly charged and the storage capacity is low. The release of energy is mainly achieved by triggering the triode by comparing the voltage of the storage capacitor C_1 with the voltage of the detection capacitor C_{in}. Fig. (c) shows the peak amplification of the storage voltage of the storage capacitor C_1 and the detection capacitor C_{in}. In Figure (c), due to the saturation characteristics of the capacitor charging and the characteristics of the triode leakage current, the capacitor voltage rise begins to have a gap. TENG outputs AC electrical signals. When the output voltage waveform decreases, the voltage in the storage capacitor C_1 will also decrease due to the leakage current characteristics of the triode. As shown in Figure (d), when the voltage of the capacitor C_1 drops to less than the voltage of the detection capacitor, due to the characteristics of the transistor conduction, the electrical energy of the storage capacitor C_1 and the electrical energy of the detection capacitor will be released. At this time, the electrical energy in the storage capacitor C_2 will also be released with the conduction of the switch. After all the electricity is released, a new cycle begins.

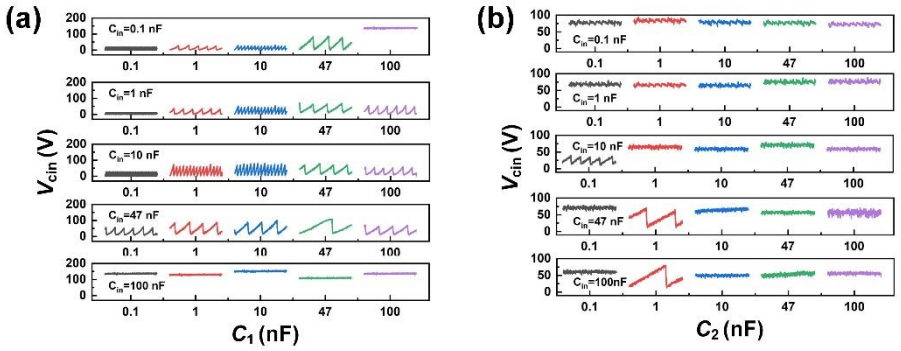

Figure S10 The voltage of Cin. (a) The voltage of Cin with different detection capacitance Cin and different storage capacitance C1 under R-TENG operation. (b) The voltage of Cin with different detection capacitance Cin and different storage capacitance C2 under V-TENG operation.

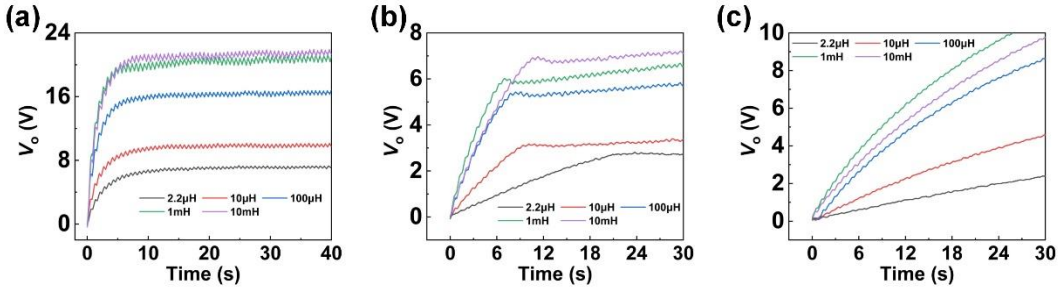

Figure S11. Output voltage plots of different types of filter inductors under (a-c) 1 μF, 22 μF and 33 μF filter capacitance conditions.

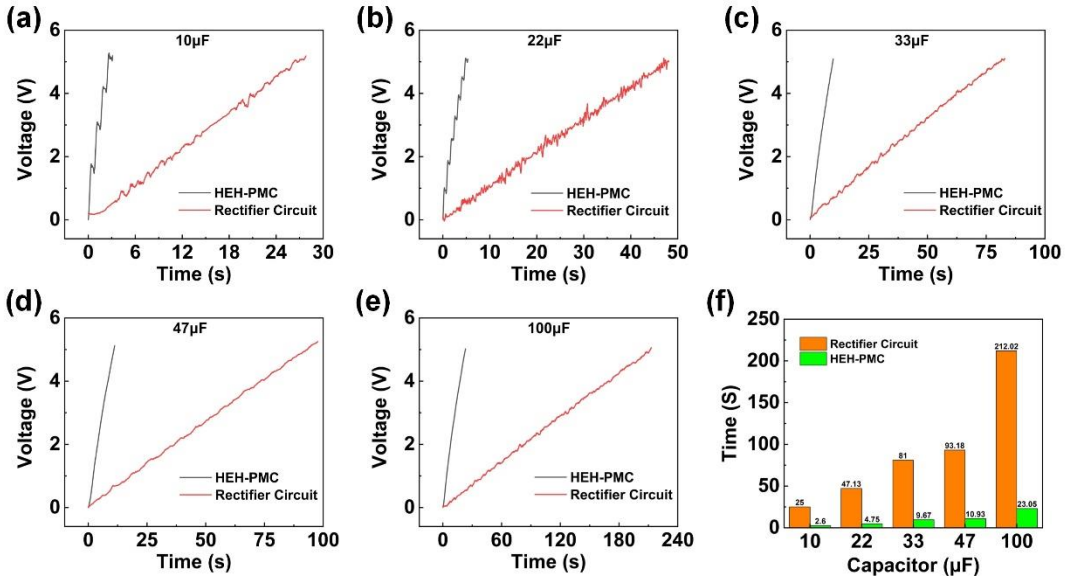

Figure S12. Voltage comparison of capacitor charging through HEH-PMC and rectifier circuit during simultaneous operation of R-TENG and V-TENG. (a-e) Charging graphs for 10 μF, 22 μF, 33 μF, 47 μF and 100 μF. (f) Plot of time taken to charge different capacitors to 5 V.

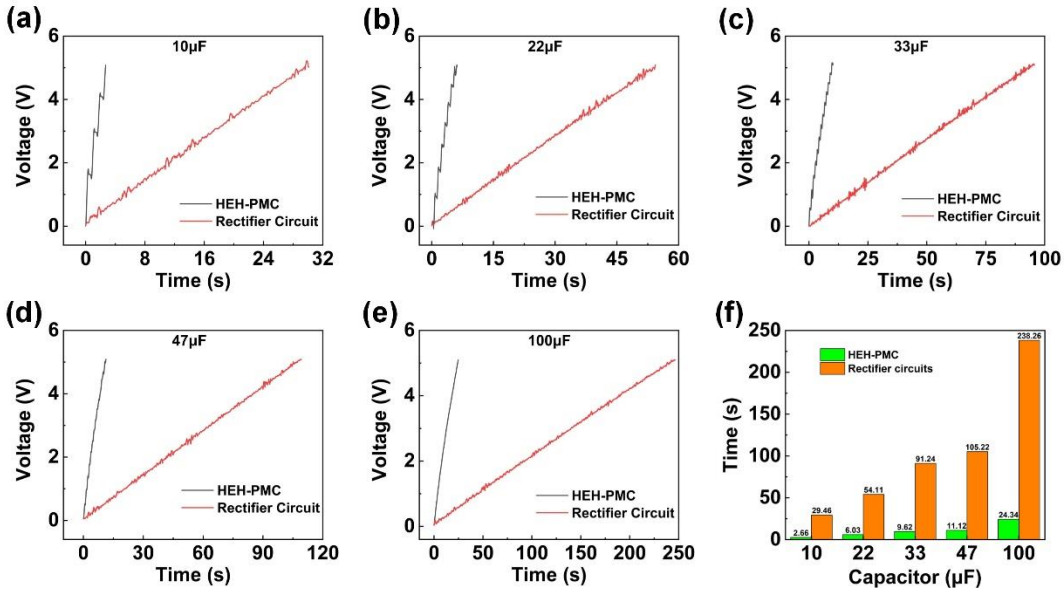

Figure S13. Voltage comparison of capacitor charging through HEH-PMC with rectifier circuit when only R-TENG is operating. (a-e) Charging graphs for 10 μF, 22 μF, 33 μF, 47 μF and 100 μF. (f) Plot of time taken to charge different capacitors to 5 V.

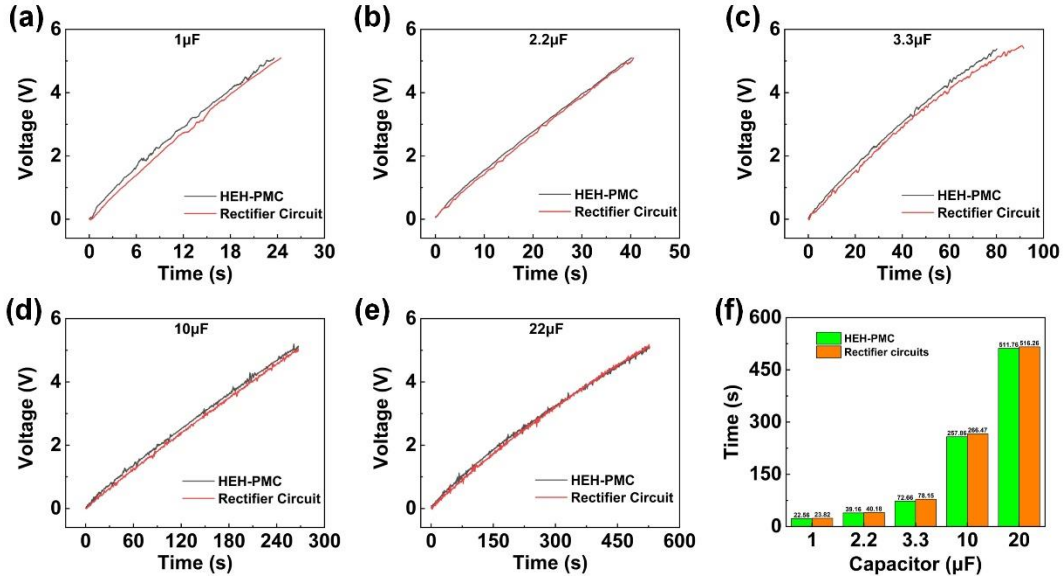

Figure S14. Voltage comparison of capacitor charging via HEH-PMC with rectifier circuit during V-TENG only operation. (a-e) Charging graphs for 1 μF, 2.2 μF, 3.3 μF, 10 μF and 22 μF. (f) Plot of time taken to charge different capacitors to 5 V.

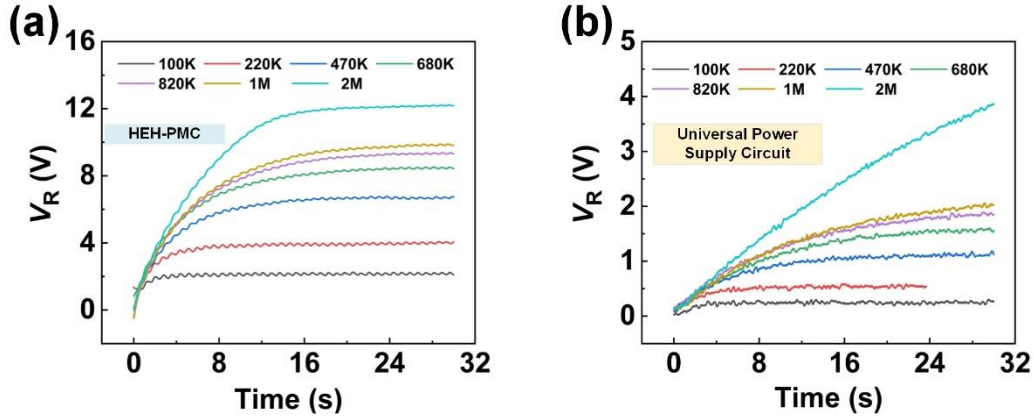

Figure S15. Voltage output curves through (a) HEH-PMC with (b) universal power supply circuit at different resistances during HEH-TENG operation.